Neural Networks 164 (2023) 464–475

Contents lists available at ScienceDirect

Neural Networks

journal homepage: www.elsevier.com/locate/neunet

Automatized offline and online exploration to achieve a target dynamics in biohybrid neural circuits built with living and model neurons

Manuel Reyes-Sanchez [a,*], Rodrigo Amaducci [a], Pablo Sanchez-Martin [a], Irene Elices [a,b], Francisco B. Rodriguez [a], Pablo Varona [a,*]

[a] Grupo de Neurocomputación Biológica, Departamento de Ingeniería Informática, Escuela Politécnica Superior, Universidad Autónoma de Madrid, 28049 Madrid, Spain
[b] Sorbonne Université, INSERM, CNRS, Institut de la Vision, 17 rue Moreau, F-75012 Paris, France

ARTICLE INFO

Article history:
Received 28 December 2021
Received in revised form 1 March 2023
Accepted 18 April 2023
Available online 26 April 2023

Keywords:
Interacting living and model neurons
Automatic parameterization
Neural sequences
Hybrid neural dynamics
Biohybrid coupling
Neurotechnology

ABSTRACT

Biohybrid circuits of interacting living and model neurons are an advantageous means to study neural dynamics and to assess the role of specific neuron and network properties in the nervous system. Hybrid networks are also a necessary step to build effective artificial intelligence and brain hybridization. In this work, we deal with the automatized online and offline adaptation, exploration and parameter mapping to achieve a target dynamics in hybrid circuits and, in particular, those that yield dynamical invariants between living and model neurons. We address dynamical invariants that form robust cycle-by-cycle relationships between the intervals that build neural sequences from such interaction. Our methodology first attains automated adaptation of model neurons to work in the same amplitude regime and time scale of living neurons. Then, we address the automatized exploration and mapping of the synapse parameter space that lead to a specific dynamical invariant target. Our approach uses multiple configurations and parallel computing from electrophysiological recordings of living neurons to build full mappings, and genetic algorithms to achieve an instance of the target dynamics for the hybrid circuit in a short time. We illustrate and validate such strategy in the context of the study of functional sequences in neural rhythms, which can be easily generalized for any variety of hybrid circuit configuration. This approach facilitates both the building of hybrid circuits and the accomplishment of their scientific goal.

1. Introduction

Biohybrid neuronal circuits are neural networks built with living and artificial neurons and connections. Their use offers broad perspectives in many fields ranging from neurobiology studies to neuromorphic engineering and the interface between implantable neuroprosthetic devices and artificial intelligence (Broccard et al., 2017; Buccelli et al., 2019; Chiolerio et al., 2017; George et al., 2020; Keren et al., 2019; Serb et al., 2020; Vassanelli & Mahmud, 2016). Although research assessing neural dynamics with this kind of circuits goes back to the early 90's and 2000's, e.g. see Le Masson et al. (1995, 2002), Nowotny et al. (2003), Oprisan et al. (2004), Potter (2002), Szücs et al. (2000), Yarom (1991), Zeck and Fromherz (2001), their use in the neuroscience community is not yet widespread. This is because hybrid circuits are, in general, rather difficult to design and implement. To establish an online connection between living cells and model neurons, either unidirectional o bidirectional, model neurons need to work at the same time regime and in many cases, in the same approximate amplitude range of cell membrane voltage. Hybrid synapses also require a realistic signaling exchange and, overall, the model dynamics needs to be compatible with that of the living cells to build an effective interaction.

Computational neuroscience models highly depend on their parameters to reproduce neural dynamics (Torres & Varona, 2012). The need for methods to establish those parameters has been long recognized, including the use of genetic algorithms (Bornholdt & Graudenz, 1992; Gonçalves et al., 2020; Keren et al., 2005; LaTorre et al., 2020; Van Geit et al., 2016; Vanier & Bower, 1999). Best parameter constraining approaches are those that involve multiple experimental validations, which also contributes to interpret the results of experimental techniques (Tennøe et al., 2018; Varona et al., 2000). Neuron and synapse models employed to build hybrid circuits require that these parameters are set

* Corresponding authors.
E-mail addresses: manuel.reyes@uam.es (M. Reyes-Sanchez), pablo.varona@uam.es (P. Varona).

https://doi.org/10.1016/j.neunet.2023.04.034

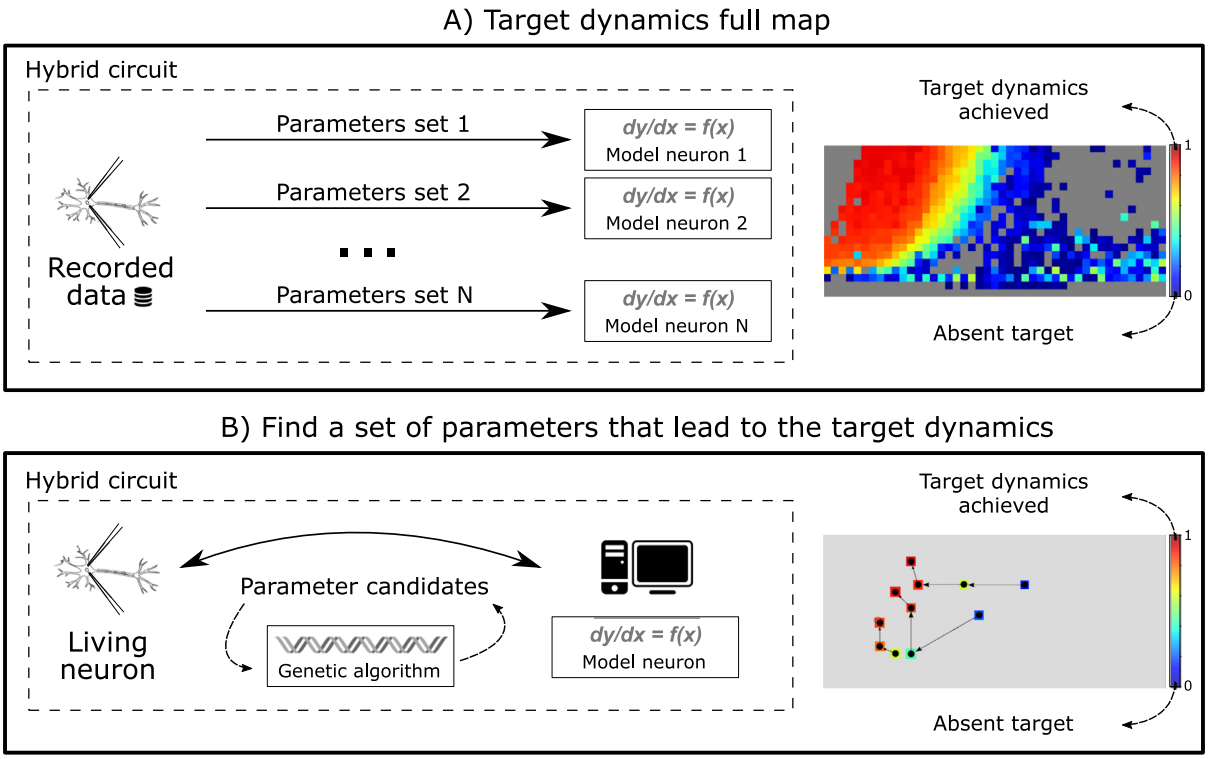

Fig. 1. Automatic model exploration approaches to achieve a target dynamics in biohybrid circuits. Panel A: building a target dynamics full map. This panel illustrates how electrophysiological recordings are input to models with continuous parameter sets and their performance to achieve a desired target dynamics is measured and mapped. The large number of simulations required can be implemented in parallel using cluster computing. Such approach leads to a full target dynamics map, but typically cannot be used in online experiments because of the long time taken by the exploration, even using optimized parallelization. Panel B illustrates a second approach in which a genetic algorithm searches iteratively over several generations for an instance of the target dynamics as characterized by a well-defined metrics. This second solution is more versatile, takes less computational resources, and can be used to tune the hybrid circuit in real-time using a bidirectional synapse. Both approaches can be combined, e.g. an online genetic algorithm search followed by validation through an offline mapping based on the experimental recordings.

during the lifespan of the hybrid circuit, which in many cases is short.

In previous works we have produced tools to ease the implementation of biohybrid circuits. In particular, we have designed algorithms to scale different neuron and synapse models to match online the dynamics of living cell recordings (Reyes-Sanchez et al., 2020). We have also released a platform that uses real-time software technology to build hybrid circuits with precise temporal constraints resulting in highly realistic interactions (Amaducci et al., 2019), and general strategies to build biohybrid closed-loop interactions (Varona et al., 2016). Algorithms that adapt model dynamics to build hybrid circuits employ calibrations based on living neuron recordings and the characterization of the effect of synaptic input both into the cells and into the models.

Biohybrid circuits typically have a well-defined goal to be completed during the experiment. Examples of such goal include the control of a living nervous system dynamics, e.g., the exploration of synaptic or neural dynamics by the interaction provided with the model neurons (Manor & Nadim, 2001), a learning target (Nowotny et al., 2003), the mapping of bifurcations in neuronal activity (Pinto et al., 2000), the control of an external device like robots, hybrots or prostheses (Kositsky et al., 2009; Soëtard et al., 2023), or driving neural activity out of a pathological state (Keren et al., 2019; Selverston et al., 2000). Most of these goals can be summarized as the achievement of a target dynamics by modifying the parameters of the interaction with model neurons.

In this work, we show that the combination of experimental recordings and theoretical paradigms can be applied to explore and rapidly tune neuron and synapse models to fulfill target hybrid circuit dynamics (see Fig. 1). The protocols that we propose here allow for the first time the automation in finding the parameter model space that results in a desired dynamics of the hybrid circuit. We illustrate this technology by searching the neuron and synaptic parameter space to yield dynamical invariants between a living cell and different model neurons connected through a graded synapse model, which mimics the current flowing into the postsynaptic cell as a function of the presynaptic membrane potential (Golowasch et al., 1999).

Dynamical invariants reflect robust sequential activations that constrain specific time intervals that build such sequences. The relationships between intervals that participate in invariants are preserved cycle-by-cycle in the sequence, underlying neural coordination even during transients (Elices et al., 2019). In our validation tests for achieving hybrid circuit target dynamics, we mapped the presence of invariants in the form of linear relationships between the interval defined by the beginning of the bursting activity between the living and model neurons and the instantaneous period of their sequence. Fig. 2 illustrates the concept of invariant showing two intervals of the sequence used in the validation examples, and the resulting linear correlation when the invariant occurs.

During the proposed protocol, we input biological time series with a characteristic temporal structure of spiking–bursting dynamics to different model neurons. The model signals and synapses are preprocessed online to automatically adapt the corresponding time and amplitude scales to those of the living neurons employed in this study. Our methodology can then map the neuron and synapse parameters that yield a dynamical invariant taking into account the temporal structure of the interaction output. By testing thousands of combinations, this approach allows a full characterization of the parameter space that contributes to

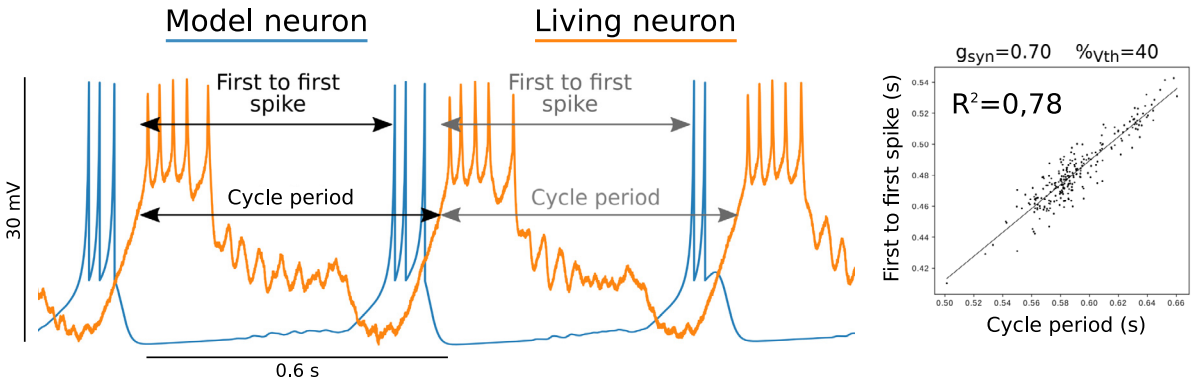

Fig. 2. Illustration of the concept of dynamical invariant in sequential neural activity. The dynamical invariant used to validate the exploration of hybrid circuit target dynamics in this paper is a linear relationship between the instantaneous period of the living neuron and the corresponding interval from the first spike of the living neuron to the first spike of the model neuron in the hybrid interaction. In addition to the implementation of the interaction between the living and model neurons, during the experiment spike events are timed and successive intervals are measured to calculate the R^2 of their correlation. The panel on the right shows an example of the correlation that defines a dynamical invariant in the sequential activations of the neurons. Each point in this panel corresponds to a cycle of the sequential interaction.

the generation of the predefined target dynamics. Because of the heavy computational task, such map typically takes up to hours to be built, and thus cannot always be implemented in bidirectional hybrid circuit preparations. Thus, we also propose the use of a genetic algorithm approach to find specific instances of the target dynamics in a few iterations. Both approaches are validated below and their combined use is discussed.

2. Experimental methods and models

2.1. Experimental methods

The experimental recordings to build hybrid circuits in this work were performed on the pyloric central pattern generator (CPG) (Marder & Calabrese, 1996; Selverston, 2005) of crustacean. Adult crabs (*Carcinus maenas*) were used in all preparations. They were purchased in a local fish shop and maintained in a tank with artificial seawater at 13-15 °C. Crabs were anesthetized by ice for 15 minutes before dissection. All procedures followed the animal treatment guidelines from the European Commission and Universidad Autónoma de Madrid. The stomatogastric nervous system was dissected and pinned in a Sylgard-coated dish containing *Carcinus maenas* saline (in mM: 433 NaCl, 12 KCl, 12 $CaCl_2 \cdot 2H_2O$, 20 $MgCl_2 \cdot 6H_2O$, 10 HEPES adjusted to pH 7.60 with 4 M 287 NaOH). After desheathing the stomatogastric ganglion (STG), neurons were identified by their membrane potential waveforms and the spike time structure observed in extracellular recordings using stainless steel electrodes from the corresponding motor nerves. Neurons' membrane potential was measured in long recordings of bursting activity from the lateral pyloric neuron using segments of 148 seconds (which included ∼180 bursts), using 3 M KCl filled microelectrodes (50 MΩ) and a DC amplifier (ELC-03M, NPI). Spikes were detected with a threshold-crossing criterion and intervals were calculated by subtracting consecutive time references. Current injection to implement hybrid connections into the living neurons (following the synaptic model described below) was delivered with a second electrode on the same neuron. Data was acquired using an A/D DAQ board (PCI-6251, National Instruments). Recordings were performed at a 10 kHz acquisition rate.

2.2. Neuron models for hybrid circuit construction

To illustrate the automation procedure to explore hybrid circuits proposed in the paper, we selected three neuronal models with distinct complexity in their dynamics. All of them can be integrated in hard real-time (Amaducci et al., 2019):

- The Izhikevich neuron model is a two-dimensional system of ordinary differential equations with a quadratic voltage nonlinearity and an after-spike reset (Izhikevich, 2003). This model can produce a wide variety of spiking activity observed in many neuron types, including the bursting behavior that we will use here to assess the presence of hybrid dynamical invariants, and it is described as:

$$dv(t)/dt = 0.004v^2 + 5v + 140 - u + I - I_{syn}$$
$$du(t)/dt = a(bv - u)$$
$$v \text{ if } \geq 30 \text{ then } \begin{cases} v = c \\ u = u + d \end{cases}$$

  The parameters used for the model bursting mode in the hybrid circuit implementation were: a=0.02; b=0.20; $c = -50$; $d = 2$; $I = 10$. In the equation for the membrane voltage v, I_{syn} is the synaptic current from the living neuron which is described below.
- The Komendatov and Kononenko (K–K) model is a biophysically realistic conductance based paradigm used to reproduce the spiking–bursting activity of different neuron types (Komendantov & Kononenko, 1996). This model can generate chaotic spiking bursting activity, which is a desirable feature in many studies that address the building up of robust neural rhythms and sequences that arise from negotiated interactions among neurons (Elices & Varona, 2015, 2017). The model description is as follows:

$$dv(t)/dt = -(\sum I_{ion} + I_{syn})/C_m$$

  where $\sum I_{ion}$ describes all ionic membrane currents and I_{syn} is the synaptic current from the living neuron explained below. The models uses the following slow-wave ionic generating mechanism for the bursting dynamics:

$$I_{Na}(v) = g^*_{Na}(v)(1/(1 + e^{-0.2(v+45)}))(v - v_{Na})$$
$$I_k = g^*_k(v - v_k)$$
$$I_{Na} = g^*_{Na}(v - v_{Na})$$
$$I_B = g^*_B m_B h_B(v - v_B)$$
$$dm_B(t)/dt = (1/(1 + e^{0.4(v+34)}) - m_B)/0.05$$

$dh_B(t)/dt = (1/(1+e^{-0.55(v+43)}) - h_B)/1.5$

The spike-generating mechanism employs the following currents:

$I_{Na(TTX)} = g^*_{Na(TTX)} m^3 h(v - v_{Na})$

$I_{K(TEA)} = g^*_{K(TEA)} n^4 (v - v_K)$

$dm(t)/dt = (1/(1+e^{-0.4(v+31)}) - m)/0.0005$

$dh(t)/dt = (1/(1+e^{0.25(v+45)}) - h)/0.01$

$dn(t)/dt = (1/(1+e^{-0.18(v+25)}) - n)/0.015$

The calcium dynamics are modeled as:

$I_{Ca} = g^*_{Ca} m^2_{Ca} (v - v_{Ca})$

$dm_{Ca}(t)/dt = (1/(1+e^{-0.2v}) - m_{Ca})/0.01$

$I_{Ca-Ca} = (g^*_{Ca-Ca}/(1+e^{-0.06(v+45)}))$

$\cdot ((v - v_{Ca})/(1+e^{k_\beta([Ca]-\beta)}))$

$d[Ca](t)/dt = \rho\{(-I_{Ca})/(2F * 4\pi R^3/3) - k_s[Ca]\}$

The parameters used in this study yield a chaotic bursting regime in the model (Komendantov & Kononenko, 1996), which will be employed to match the variability observed in living neurons (Elices et al., 2019) for the hybrid circuit implementation:

$C_m = 0.02$ μF; $g^*_{Na} = 0.023$ μS; $g^*_k = 0.25$ μS; $g^*_B = 0.165$ μS; $g^*_{Na}(v) = 0.11$ μS; $v_k = -70.0$ mV; $v_B = -58.0$ mV; $v_{Na} = 40.0$ mV; $g^*_{Na(TTX)} = 400.0$ μS; $g^*_{Ca} = 1.5$ μS; $k_\beta = 15000.0/$ mM; $g^*_{K(TEA)} = 10.0$ μS; $v_{Ca} = 150.0$ mV; $\beta = 0.00004$ mM; $g^*_{Ca-Ca} = 0.02$ μS; $k_s = 50.0/$ s; $\rho = 0.002$; $F = 96.485$.

- Finally we use the Ghigliazza and Holmes model, a conductance model with the sigmoid voltage dependencies of the classic Hodgkin–Huxley descriptions (Ghigliazza & Holmes, 2004), which is described by the following equations:

$dv(t)/dt = -(\sum I_{ion} + I_{syn})/C_m$

$dm(t)/dt = (\epsilon/\tau_m)(1/(1+e^{-k_K(v(t)-v_{th\_K})}) - m(t))$

$dc(t)/dt = (\delta/\tau_c)(1/(1+e^{-k_{Ks}(v(t)-v_{th\_Ks})}) - c(t))$

and the following ionic current descriptions:

$I_{Ca} = g_{Ca}(v(t) - E_{Ca})/(1+e^{-k_{Ca}(v(t)-v_{th\_Ca})})$

$I_l = g_l(v(t) - E_l)$

$I_k = g_K m(t)(v(t) - E_K)$

$I_{k_s} = g_{Ks} c(t)(v(t) - E_K)$

The parameters used for the hybrid circuit implementation of this model were set in the bursting regime (Ghigliazza & Holmes, 2004):

$g_{Ca} = 4.4$ mS/cm^2; $E_{Ca} = 120$ mV; $v_{th\_Ca} = -1.2$ mV; $k_{Ca} = 0.11$ mV/s; $g_K = 9$ mS/cm^2; $E_K = -80$ mV; $v_{th\_K} = 2.0$ mV; $k_K = 0.2$ mV/s; $g_{Ks} = 0.25$ mS/cm^2; $v_{th\_Ks} = -27$ mV; $k_s = 0.8$ mV/s; $g_l = 2.0$ mS/cm^2; $E_l = -60$ mV; $C_m = 1.2$ μF/ cm^2; $I = 35.6$ mV.
We used a fixed time constant $\tau_m = \tau_c = 0.8$.

Each model has its own particular bursting characteristics, level of adaptability for the hybrid circuit dynamics and specific computational cost. This allowed us to test how the target goal for the hybrid circuit depended on the chosen neuron model.

2.3. Synapse model for hybrid circuit construction

To connect the living and model neurons we used a model of an inhibitory chemical graded synapse, which is a common synaptic interaction underlying the sequential activations of most known central pattern generator circuits (Golowasch et al., 1999). In this type of synapses, neurotransmitters are released progressively from a threshold value of the presynaptic membrane potential, which is lower than the spike amplitude. Thus, the amplitude of the current resulting from this type of synapse depends both on the presynaptic and postsynaptic neuron voltages. Mutual inhibition with this type of synapses typically leads to regularized sequential activations (Elices et al., 2019; Varona et al., 2001). The current injected in the models is described by the following equation:

$I_{fast} = g_{fast}(V_{MN} - E_{syn})/(1+e^{s_{fast}(V_{th}-V_{LN})})$

The default parameters for the synapse were: $g_{fast} = 0.6$ and $s_{fast} = 5$.

For the bidirectional experiments we also implemented a slow graded synapse from Golowasch et al. (1999), by injecting the following current into the living cell:

$I_{slow} = g_{slow} m(V_{LN} - Esyn)$

$dm(t)/dt = (k_1(1-m)/(1+e^{s_{slow}(V_{th}-V_{MN})})) - k_2 m$

The default parameters for the synapse were: $g_{slow} = 0.6$, $k_1 = 1.0$, $k_2 = 0.03$, $s_{slow} = 1$. All hybrid synapses were implemented using the dynamic clamp technique (Nowotny & Varona, 2014).

To avoid the effect of voltage drift during the experimental recordings, we did not employ a fixed value of E_{syn} and V_{th}, but instead used a technique proposed in Reyes-Sanchez et al. (2020) where these values are calculated as a percentage of the specific voltage range of the signal evaluated in every cycle. In particular, the default percentages applied were: $E_{syn} = 15.0\%$ and $V_{th} = 32.0\%$.

Note that building hybrid interactions requires scaling the living neuron voltage (V_{LN}) to the working regime of the model, adjusting the model time constants to match the living neuron and model dynamics, and calculating the optimal threshold and reversal potentials (V_{th} and E_{syn}). For such tasks, we used the algorithms described in Reyes-Sanchez et al. (2020), which allow the automatic calibration and adaptation of the different working regimes of neuron models to those of the biological cells. These algorithms also managed the integration of the model neurons, allowing to match the input data flow and the speed of output production with the sampling frequency of the electrophysiological recordings. The online detection of the events by which the presence of the dynamical invariant is evaluated (spike detection and the assessment of their category as first of last spikes in a burst and the quantification of the corresponding intervals and instantaneous cycle period, see Fig. 2) was also performed online.

For the integration of the differential equations a 6(5) order Runge–Kutta numerical method was used (Hull et al., 1972).

2.4. Full map exploration

Full map exploration requires quantifying the metrics for the target goal in a specified range of parameters controlling the biohybrid interaction. Bidirectional hybrid interactions require an online protocol which can take longer than the lifespan of the preparation. However, in monodirectional hybrid circuits, where the model neuron receives input from the living neuron but does not send any feedback, the exploration for the presence of dynamical invariants can be processed offline from the electrophysiological recordings. Thus, intracellular neuronal recordings are used as input to the model neurons and different model parameters can be tested to evaluate the presence of dynamical

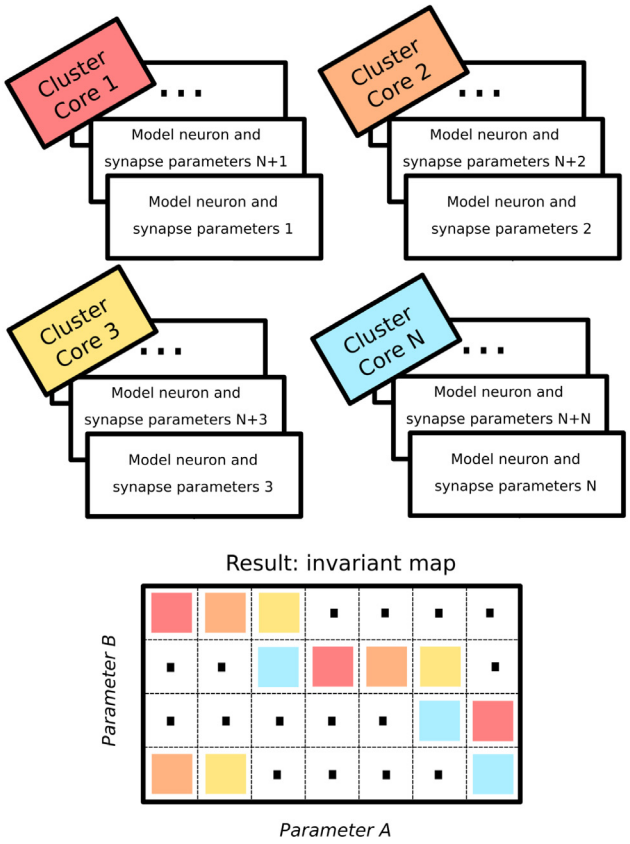

Fig. 3. Parallelization strategy to produce the target dynamics map in a biohybrid circuit. Each core simulates a batch of different configurations. The resulting map integrates all the partial results computed at each core. The colors indicate how each cell of the target map is assigned to a different cluster core. Input data from the electrophysiological recording is shared by all processors.

invariants with any arbitrary resolution for the search. The activity of the living neuron can be delivered through the model synapse into multiple versions of a neuron model as illustrated in Fig. 3. This allowed to parallelize multiple configurations to build full maps of the target dynamics in the model parameter space. Since this process is computationally expensive when the parameter space is wide and/or high resolution for the map is used, high performance cluster computing can be employed for this task.

This approach allows to save time, reducing the cost of evaluating the parameter space from 1–2 days to 2–3 hours (see Table 1 for a comparison of the performance of the different search strategies). Fig. 3 shows how the work was distributed through the different cores available. The target dynamics map was built from the different experiments distributed throughout the cluster cores. In this study, we used nodes with AMD EPYC 7451 processors, splitting the work across hundreds of nodes, e.g. for a 900 grid cell map, 180 cores were used, each node executing 5 cells.

2.5. Genetic algorithm

In hybrid-circuit online protocols, and particularly in those cases in which bidirectional interaction between living and model neurons is required, time needed to achieve the target dynamics is a crucial element. Therefore, full map explorations are not typically an option in these situations due to the long time required to build them. For these cases, we designed an online protocol that employs a genetic algorithm to search for model parameters that lead to an instance of the target dynamics. This approach does not yield a complete map of the parameter space or a confirmation that the final result is fully optimal but we determine a minimum level of performance for the target dynamics. We have implemented a genetic algorithm that randomly creates a population consisting of a set of individuals with different parameters for the biohybrid interaction. For each individual experiment, ongoing online offset and amplitude adaptations are performed and the target is evaluated using a cost function. This function assesses the presence of the target dynamics and measures its performance. Using such score, we save the best individual for the next generations (elite) and create new individuals mixing the parameters of the current individuals (crossover). The crossover process takes into account the cost function, correlating the probability of mixing each individual to the obtained score. The algorithm also introduces random variations in the parameters (mutation) to increase the variability and obtain better results. This approach only takes a few minutes (see Table 1), which makes it highly convenient for biohybrid circuits built with bidirectional synapses.

In the examples shown below, we chose a single elite individual from a reduced population of individuals and generations to yield a fast evolution. For the crossover process, individuals with score 0 were not taken into account. Random genes from individuals with score $>$ 0 where selected to create new individuals in each generation. The mutation process was applied to all new individuals by modifying the genes following a uniform distribution. Other configurations can also be used to balance the resulting increase in the accuracy and the time taken to evolve the parameter search from the choice of individual, generation and mutation numbers and strategies. The process followed the algorithm described below:

```
Define number of individuals and generations
Set duration of the hybrid interactions
Random creation of the initial population
Initial signal range & time calibration
During i generations:
    For each individual j in population:
      Hybrid Experiment on individual j:
        Ongoing offset & amplitude adaptations
        Voltage read & event detection
        Synapse computation
        Current injection
      Cost function score for individual j
    Sort population by individuals score
    Save elite individual
    Crossover individuals
  Mutate individuals
```

In the monodirectional validation experiments we created a population of three individuals, with one elite individual across four generations. In these first experiments, the complete maps were also produced, and we compared both methods to check if the genetic algorithm found an optimal set of parameters. In the online experiment, each generation required a substantial amount of time. For this reason, in the online experiments with living neurons, we used three generations. The validation shows that this number of generations is enough to obtain a good result. See Results section for more details.

For a dynamical invariant target, the cost function used was the linear correlation R^2 between the two intervals defined in Fig. 2 calculated as follows:

Table 1
Differences between the two discussed approaches for the search of target dynamics in hybrid circuits in terms of online and offline nature, exploration technology, time taken, and technology needed.

Mode	Goal	Exploration strategy	Time	Technology needed
Offline	Parameter space mapping	Serial map exploration	Very slow (1–2 Days)	Standard PC
		Parallel map exploration	Slow (2–3 Hours)	Computer cluster
Online (Real-time constraints)	Find one valid configuration	Genetic Algorithm	Fast (Minutes)	Fast CPU, GPUs

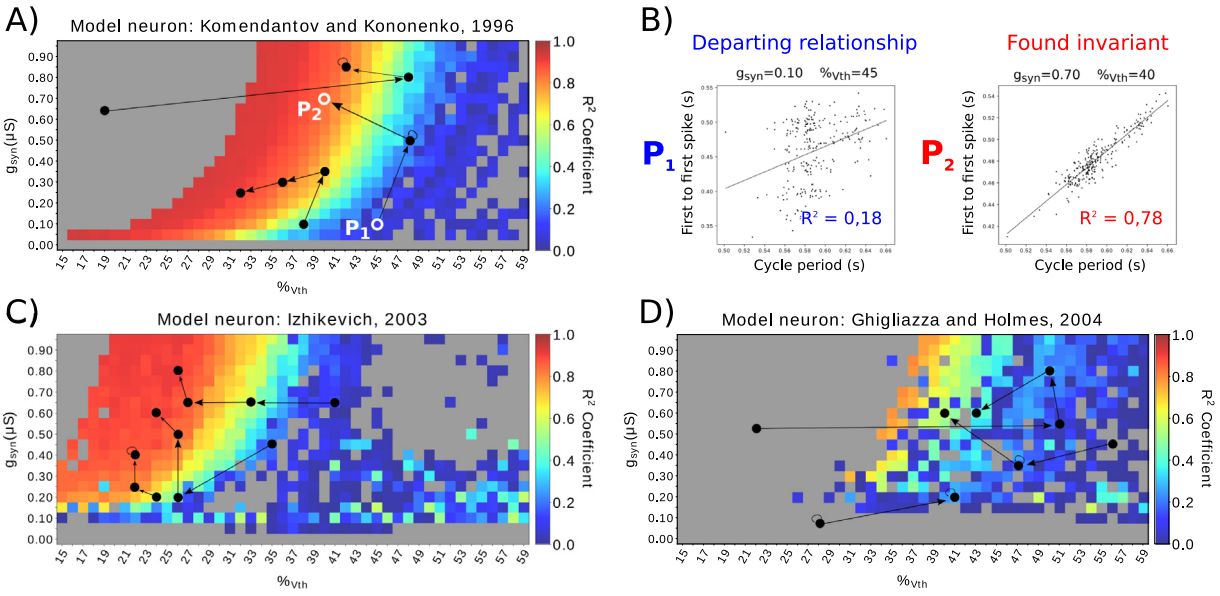

Fig. 4. Synaptic conductance vs. graded synapse threshold exploration in monodirectional hybrid circuits. In this figure, we assess how the synaptic conductance to the model neuron and the voltage threshold of the synapse affect the emergence of the dynamical invariant in three distinct neuron models (panels A, C and D). The threshold parameter V_{th} is calculated for each model regime, thus here is represented as a percentage of the range of the total voltage signal. The conductance g_{syn} is measured in μS. Trajectories indicated by black dots and arrows represent distinct evolutions of the genetic algorithm in search of the target dynamics, and are superposed over the full maps for their validation. Each model neuron panel shows three different trajectories (indicated with arrows) from randomly selected points and their final destination. Each black point represents the best individual for that iteration of the genetic algorithm. Autoloop lines represent an exploration where new generations had no better individuals created, and thus the best set of parameters corresponded to the current elite. Panel B shows an illustrative example of the interval relationships for the Komendantov and Kononenko model, corresponding to the departing parameters and the final parameters of one execution of the genetic algorithm. The first set of parameters, completely random, has a very low R^2 value, while the final set yields correlated intervals, showing that the target dynamics was achieved in the hybrid circuit.

$$R^2 = \frac{Covariance(x,y)^2}{Variance(x)^2 Variance(y)^2}$$

where x is the living neuron's cycle period and y is the first-to-first spike interval, as is illustrated in Fig. 2.

3. Results

3.1. Full map exploration

Representative examples of full parameter exploration and mapping of hybrid circuit dynamics that lead to dynamical invariants are shown in Figs. 4, 6, and 7. The color code in each map indicates the resulting R^2 correlation value for each model neuron and set of tested parameters as specified in the map axis. The regions colored in red or orange correspond to a strong presence of the dynamical invariant ($R^2 > 0.75$). A weak dynamical invariant is represented in yellow or green tones ($0.5 < R^2 < 0.75$). Different tones of blue indicate that the invariant is absent ($R^2 < 0.5$) for that particular region of the parameter space. Gray color is used to indicate when the set of parameters does not result in robust rhythms with sequential cyclic activation of the neurons. This behavior can occur mainly because of two reasons: (i) the amount of current injected into one neuron from the other can be too large and thus resulting in complete inhibition of the neural activity, or (ii) not enough to create the joint rhythm. The time course of the interaction currents as a function of the ongoing dynamics of the neurons yields the level of correlation between the two explored intervals that build invariants.

Fig. 4 illustrates the effect of voltage threshold (V_{th}) and synapse conductance (g_{syn}) on the presence of the dynamical invariant for three types of neuron models studied. Panel 4A shows the results obtained using a Komendantov–Kononenko model neuron. This model has high flexibility in the hyperpolarization and good adaptability in burst duration from the interaction with the living neuron resulting in large regions with dynamical invariants, as illustrated by the wide red to orange zones in the map. Panel 4B shows two representative points from the map depicted in panel 4A. P_1 corresponds to a disperse cloud of points in the relationship between the instantaneous period and the first-to-first spike interval and thus the linear correlation obtained is low ($R^2 = 0.18$). On the other hand, P_2 corresponds to an example of parameter combination that leads to the searched relationship with large correlation between the instantaneous period and the first-to-first spike interval ($R^2 = 0.78$). Panel 4C shows the results

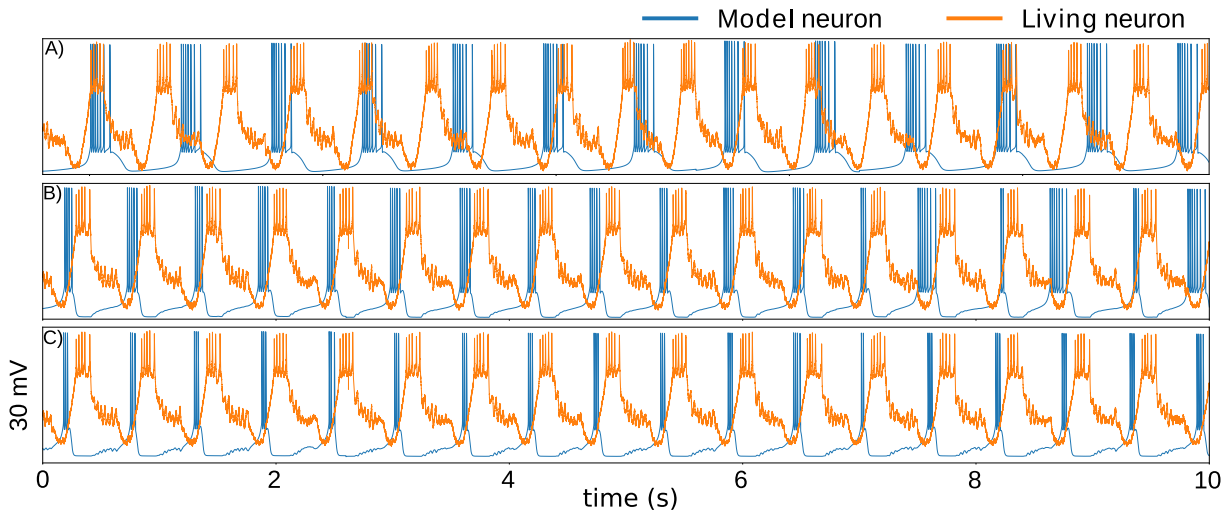

Fig. 5. Representative time series of the monodirectional interaction between the living (orange) and K–K model (blue) neurons in a hybrid circuit for the three distinct regions in the maps depicted in Fig. 4A. Panel A corresponds to a region of the parameter space in which no robust sequential activation is achieved (gray regions in the maps, signals from Fig. 4A, cell $\%_{Vth} = 58$ and $g_{syn} = 0.30$, $R^2 = 0.0$). Panel B corresponds to a region with a robust sequential activation but no invariant (blue regions in the maps, signals from Fig. 4A, cell $\%_{Vth} = 45$ and $g_{syn} = 0.10$, $R^2 = 0.12$). Panel C corresponds to a robust invariant (orange-red regions in the maps, signals from Fig. 4A, cell $\%_{Vth} = 32$ and $g_{syn} = 0.25$, $R^2 = 0.9$). The mean period of the living neuron in this recording was 0.59s and coefficient of variation $C_v = 0.043$. The model signal in panel A had different metrics, with a mean period of 0.77s and coefficient of variation $C_v = 4.0e^{-5}$. In Panel B the mean period of the model neuron matched the period of the living mean period with 0.59s but with a different coefficient of variation $C_v = 0.15$. Finally, in panel C, the model neuron exhibited metrics almost equal to the living neuron, with a mean period of 0.59 s and a coefficient of variation $C_v = 0.045$. The amplitude of these signals is 30 mV.

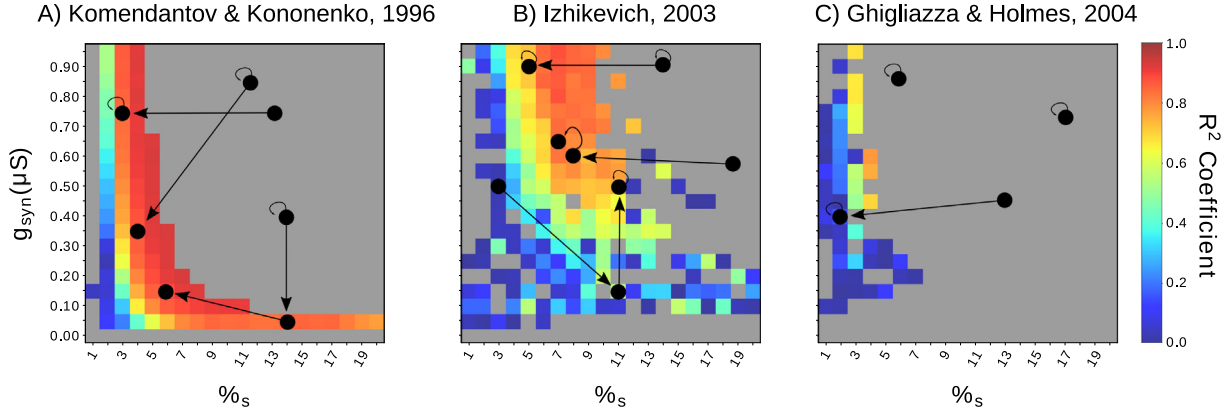

Fig. 6. Exploration of the synaptic conductance vs. the parameter *s* that scales the presynaptic potential and release threshold of the monodirectional hybrid chemical synapse. Differences in the presence of the invariant can be observed between model neurons. When the colored area occupies a small area of the complete map, like in the Ghigliazza and Holmes model map, the genetic algorithm can get stuck in a gray zone (no sequential rhythm present). Example trajectories of the genetic algorithm indicated by the arrows are superposed in the full map for their validation.

of the same experiment performed with the Izhikevich neuron model. While the map trend is similar, it is shifted to the left, since the Izhikevich neurons need more current injection than Komendantov and Kononenko neurons to be affected by the living neuron, therefore for this model the voltage threshold to find the invariant is lower. However, in panel 4D we can see that using a Ghigliazza and Holmes model neuron it is not possible to obtain a clear region that leads to a robust presence of the dynamical invariant, and only a few values of the parameter space seem to be close to the target goal.

Fig. 5 shows representative time series of the activity resulting from the interaction in the hybrid circuit for the three regions discussed in Fig. 4. Note that the dynamical invariants are only present when the interaction results in robust sequential activity between the neurons and the level of variability of the intervals in the living cell is matched by the variability in the model neuron.

In Fig. 6 we map the *s* parameter of the synapse model, which scales the difference between the release threshold voltage and the presynaptic potential (see Section 2.3), against the maximum synaptic conductance. Comparing the results in panels A and B for Komendantov and Kononenko and the Izhikevich model, respectively, we observe that the former neuron model has a stronger presence of the dynamical invariant, with wider parameter areas close to $R^2 = 1$ than the Izhikevich model, which nevertheless displays several regions with high correlations. Despite of this, the Izhikevich model offers more possible combinations of parameters that lead to robust sequential activations from the interaction (colored areas). Ghigliazza and Holmes model neuron offers neither a wide area of robust sequential interaction nor a strong presence of the invariant with the chosen model parameters.

In Fig. 7, we explored at the same time V_{th} and *s*. Similar results to those in Fig. 6 were obtained, as wide and continuous areas of the map with a high presence of the dynamical invariant were present for the Komendantov and Kononenko model (panel A) and more colored areas, but with lesser high correlation were

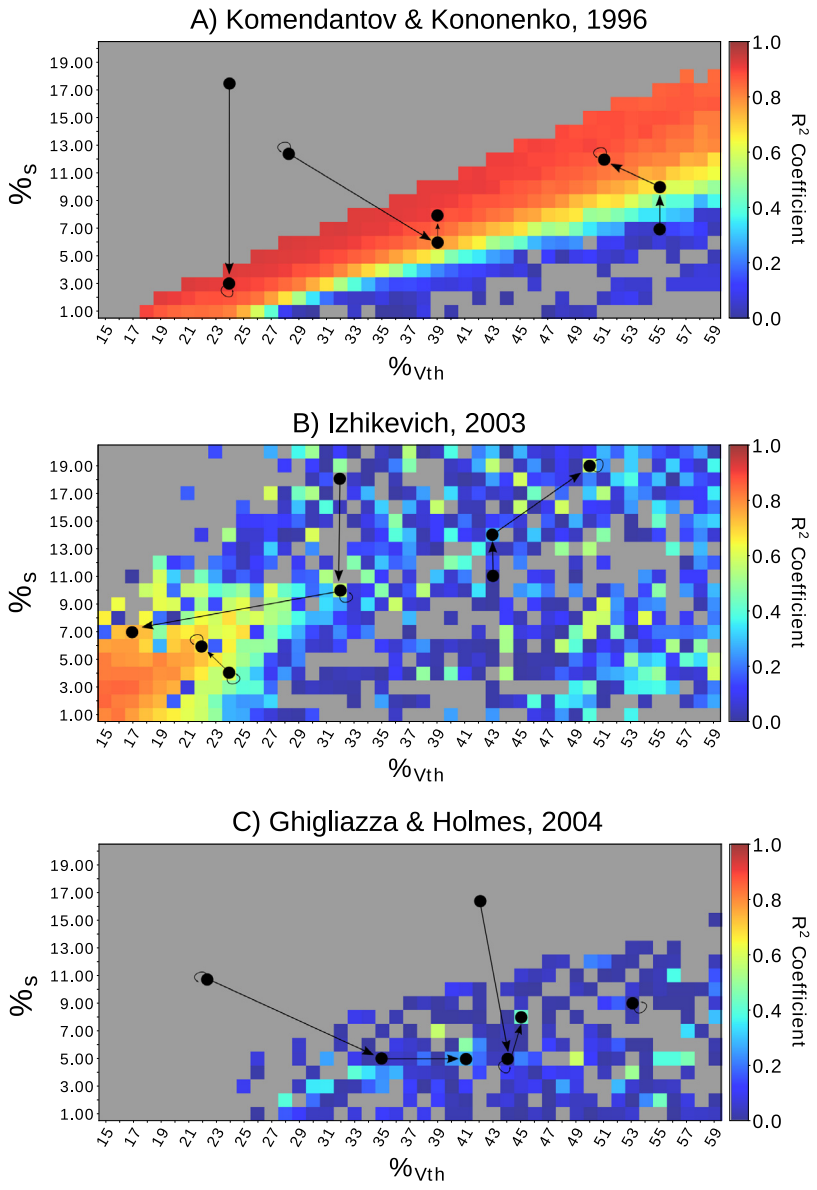

Fig. 7. Maps of the presence of the dynamical invariant (R^2 Coefficient) when the s parameter and the voltage threshold V_{th} of the monodirectional graded chemical synapse used are explored. As in the previous figures, parameters s and V_{th} are represented as a percentage of the range of the voltage signal. While for the Komendantov and Kononenko model there is a widespread presence of the dynamical invariant, the Izhikevich model shows a different shape for the regions in which the dynamical invariant is present, mainly concentrated for low values in both axes. From the combination of these two parameters, and although it is possible to achieve a valid rhythm between both neurons (colored zones), the Ghigliazza and Holmes model does not yield dynamical invariants (orange to red zones absent). Example trajectories of the genetic algorithm indicated by the arrows are superposed in the full map for their validation.

present for Izhikevich model (panel B). Finally, the Ghigliazza and Holmes model has the worst results and could not achieve the target dynamical invariant (panel C). With the chosen parameters for the time constants of m and c, this model has a more restricted capability to follow the dynamics from the living neuron after the hyperpolarizations than the Komendantov–Kononenko and Izhikevich models.

3.2. Genetic algorithm target dynamics search

As we have discussed in the previous sections, the genetic algorithm can be used to perform a fast informed search instead of calculating all possible parameter combinations to explore the target dynamics full map. The genetic algorithm searches for the target dynamics using a restricted set of invariant evaluations, plotted as dark points over the complete maps in Figs. 4, 6 and 7. These points are linked through lines with arrows in these figures to indicate the trajectory followed by the genetic algorithm search. In each figure, three illustrative trajectories show how the genetic algorithm progressively finds a set of parameters with higher R^2 for the linear correlation value of the target dynamics.

This protocol helps to select which model is more reliable to reproduce the dynamical invariant in ongoing experiments. Complete maps help us to evaluate offline which models yield wider parameter ranges that reproduce the target dynamics, while the genetic algorithm is a useful tool to readily achieve the target dynamics during an ongoing experiment.

Note that the results of the search for dynamical invariants are different for each model used to build the hybrid circuits. This was expected as each model has its own specific bursting characteristics and level of adaptability for the hybrid circuit dynamics based on the synaptic interactions. The Komendantov–Kononenko model displayed the best combination of intrinsic

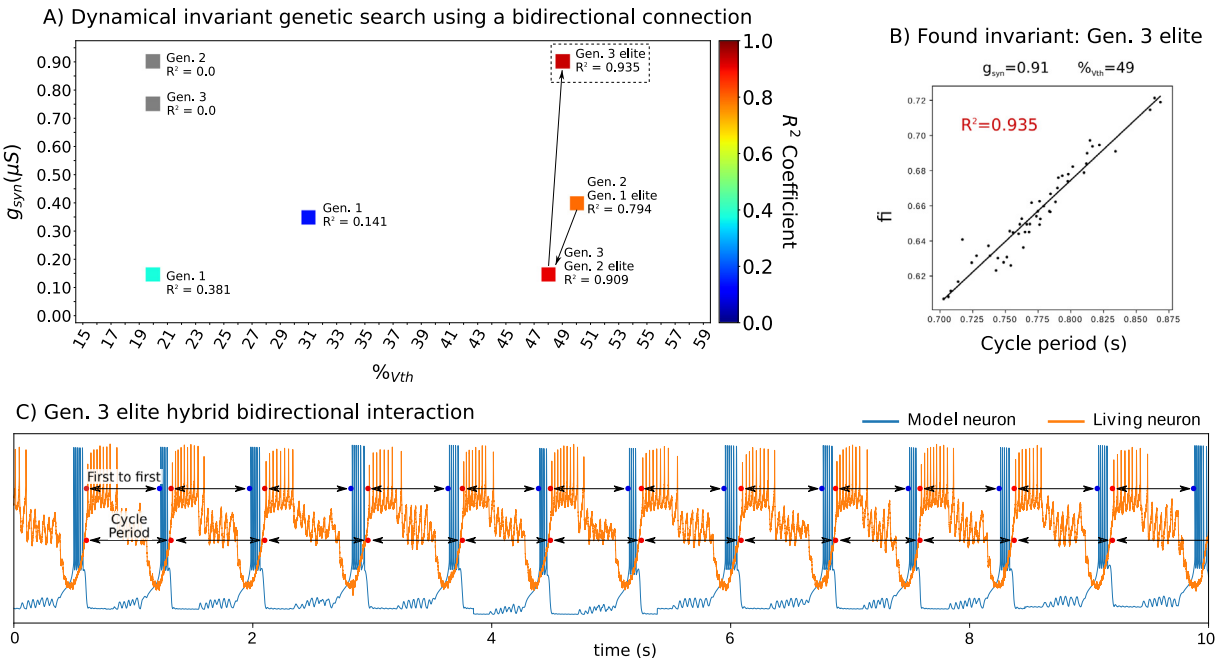

Fig. 8. Representative illustration of online synaptic tuning with a genetic algorithm of a bidirectional hybrid circuit. This experiment was performed in real time with a living preparation with a bidirectional connection from and to the living cell using real-time software technology. Panel (A) shows the online evolution of the genetic algorithm which is able to find the dynamical invariant in three generations. The best individual of each generation is marked as elite and linked with arrows. The other individuals correspond to intermediate stages in each generation. Panel (B) shows the resulting dynamical invariant for the final elite individual. Panel (C) shows the time series of the bidirectional interaction with the living neuron for this final elite. The real-time detection of the time references used to calculate the invariant from the first-to-first interval and instantaneous period are indicated in black. The amplitude of the signal is 30 mV.

variability in the neuron dynamics and adaptation to the inhibitory interaction to build dynamical invariants.

Bidirectional interactions between living and model neurons in hybrid circuits can more effectively lead to the target dynamics than monodirectional hybrid circuits. Fig. 8 illustrates this in a bidirectional interaction between a pyloric LP neuron and a Komendantov–Kononenko model neuron. The synapse from the LP cell to the model neuron was modeled with the fast graded model used in the previous monodirectional examples. The synapse from the model neuron to the living cell was implemented with the slow synapse paradigm described above to mimic the PD-LP neuron interaction in the pyloric CPG (Golowasch et al., 1999).

Panel A in Fig. 8 shows the evolution of the genetic algorithm within this bidirectional hybrid circuit interaction. Arrows indicate the transit in the evaluation of the dynamical invariant between elite individuals in consecutive generations. Representative examples of intermediate individuals are also shown in this panel. Note that the genetic algorithm is able to find a robust invariant with $R^2 = 0.935$ in just three generations. The corresponding monodirectional map in this preparation, built with the same protocol as the previously discussed, yields a maximum $R^2 = 0.73$. In all our experiments, bidirectional interactions were more effective to find dynamical invariants than monodirectional protocols. Fig. 8A also illustrates that intermediate individuals within a generation often yield worst invariant results during the exploration than the previous elite. The overall target dynamics search in this example took 18 minutes with 90 second interaction intervals to quantify the relationships that built the invariant for each individual. Panels B and C show the final dynamical invariant achieved and a section of the corresponding time series of the resulting interaction.

The supplementary video shows further details of the evolution of the target dynamics exploration. The video illustrates the real-time quantification of the dynamical invariant for each generation elite together with the ongoing time series of the bidirectional interaction between the living and model neurons (Appendix A).

4. Conclusions

Biohybrid circuits that use interacting living and model neurons are key tools to study neural dynamics and to assess the role of specific neuron and network properties in emergent phenomena of neural computation. However, hybrid circuits are not easy to design nor to implement because of the inherent difficulty underlying the interaction between living and model neural dynamics, and the associated technical issues. In this work, we assessed the automation of the exploration and mapping of model parameters in hybrid circuits and, in particular, those that yield dynamical invariants as an illustration of well-defined target dynamics in the interaction between living and model neurons.

We first adapted the model neurons to work in the same amplitude regime and time scale of living neurons. Then, we automatically explored and mapped different combinations of the synapse parameter space which lead to achieve a specific dynamical invariant target. Our approach used multiple configurations and parallel computing from the same input time series of living neurons to build full mappings. We illustrated this methodology in the context of the study of dynamical invariants defined as preserved cycle-by-cycle relationships between specific time intervals that build robust sequences in neural rhythms. The existence of such invariants in the pyloric CPG of crustacean has been recently unveiled, even under the presence of intrinsic or induced large variability in the rhythms (Elices et al., 2019). Robust invariants shaping the coordination of sequential neural activity can be present in a wide variety of nervous systems, which can be a source of bioinspiration for the development of novel artificial intelligence, autonomous robotics and rehabilitation protocols (Elices et al., 2019; Garrido-Peña et al., 2021). The proposed strategy can be employed in any hybrid circuit

consisting of many types of neural recordings and models. In this work, we built the biohybrid circuit with current synaptic models implemented with dynamic clamp, but the same approach can be generalized with other techniques for the interaction such as neurotransmitter or neuromodulator microinjection or optical stimulation (Chamorro et al., 2012; Shi et al., 2021).

We also showed that a genetic algorithm can readily lead to finding the target dynamics in a few minutes. This approach was validated by contrasting this fast exploratory search with full maps, which due to the extensive search can take several hours to be completed, and thus cannot be used for online hybrid circuit experiments. The genetic algorithm approach leads to the invariant in a few minutes and is adequate for real-time hybrid experiments including bidirectional interactions between living and model neurons. In general, bidirectional interactions between living cells and model neurons are more effective to find the invariant target dynamics than monodirectional protocols.

The code to implement the map exploration and the genetic search is available at the following links:

- https://github.com/GNB-UAM/RTHy_mono
  Map exploration code: A version of RTHybrid modified to work offline with living neurons recordings, used to create the complete maps in this paper (Figs. 4, 6 and 7).
- https://github.com/GNB-UAM/RTHy_genetic
  Genetic algorithm code: Standard RTHybrid with the addiction of the code that controls the genetic algorithm. The genetic algorithm code, in python, creates XML configuration files for RTHybrid and automatically launches the experiments to perform the needed hybrid circuits. This code was employed in the online bidirectional hybrid circuit built with the living neuron showed in Fig. 8.

The repositories content additional information about how to use them. The code can be easily generalized for the exploration of other neuron and synapse parameters, including distinct target dynamics evaluated from the spiking activity of living and model neurons.

The hybrid scientific approach and tools described in this paper can be used to assess a wide variety of neuronal and synaptic dynamics phenomena, which are currently assessed separately or exclusively in experimental and modeling efforts. These phenomena include the long standing domain of synchronization (Puebla et al., 2017; Zirkle & Rubchinsky, 2021), and also novel research on inverse resonance (Torres et al., 2020b), vibrational resonance (Calim et al., 2021), neural sequence processing (Torres et al., 2020a), history-dependent excitability (Baroni et al., 2010), etc.

Although the synergy between simulation, parallel computing, optimization and artificial intelligence has been emphasized in many different scientific areas (Melab et al., 2020), their joint use in hybrid circuit construction and associated applications has not been exploited so far. In this paper we have presented a first approach in this context. Neuronal and synapse models are typically developed under the intrinsic constraint of being simple and adapted to the current knowledge under which they were developed. The dynamical richness of their living counterparts is only captured partially. Protocols that explore the dynamical range in which such models can be used to implement biohybrid circuits are very much needed in experimental neuroscience. This is the path to design effective biohybrid circuits with compatible dynamics of living and model neurons, which not only require technological development (Frank et al., 2019; Musk, 2019; Rochford et al., 2020; Serb et al., 2020; Wan et al., 2020; Xia et al., 2021; Zaer et al., 2021), but also understanding of coordination dynamics even at the level of single neuron and small circuits. Such methodology can lead to future disruptive technologies of hybrid brains in the context of implant neurotechnology.

Declaration of competing interest

The authors declare that they have no known competing financial interests or personal relationships that could have appeared to influence the work reported in this paper.

Data availability

Data will be made available on request

Acknowledgments

This research was supported by grants AEI/FEDER PID2021-122347NB-100, PGC2018-095895-B-I00, and PID2020-114867RB-I00 (funded by MCIN/AEI/10.13039/501100011033 and ERDF - "A way of making Europe").

Appendix A. Supplementary data

Supplementary material related to this article can be found online at https://doi.org/10.1016/j.neunet.2023.04.034.

References

Amaducci, R., Reyes-Sanchez, M., Elices, I., Rodriguez, F. B., & Varona, P. (2019). RTHybrid: A standardized and open-source real-time software model library for experimental neuroscience. *Frontiers in Neuroinformatics*, *13*, 11. http://dx.doi.org/10.3389/fninf.2019.00011.

Baroni, F., Torres, J. J. J., & Varona, P. (2010). History-dependent excitability as a single-cell substrate of transient memory for information discrimination. *PLoS One*, *5*(12), Article e15023. http://dx.doi.org/10.1371/journal.pone.0015023.

Bornholdt, S., & Graudenz, D. (1992). General asymmetric neural networks and structure design by genetic algorithms. *Neural Networks*, *5*(2), 327–334. http://dx.doi.org/10.1016/S0893-6080(05)80030-9.

Broccard, F. D., Joshi, S., Wang, J., & Cauwenberghs, G. (2017). Neuromorphic neural interfaces: from neurophysiological inspiration to biohybrid coupling with nervous systems. *Journal of Neural Engineering*, *14*(4), 41002. http://dx.doi.org/10.1088/1741-2552/aa67a9.

Buccelli, S., Bornat, Y., Colombi, I., Ambroise, M., Martines, L., Pasquale, V., Bisio, M., Tessadori, J., Nowak, P., Grassia, F., Averna, A., Tedesco, M., Bonifazi, P., Difato, F., Massobrio, P., Levi, T., & Chiappalone, M. (2019). A neuromorphic prosthesis to restore communication in neuronal networks. *iScience*, *19*, 402–414. http://dx.doi.org/10.1016/j.isci.2019.07.046.

Calim, A., Longtin, A., & Uzuntarla, M. (2021). Vibrational resonance in a neuron-astrocyte coupled model. *Philosophical Transactions of the Royal Society of London A (Mathematical and Physical Sciences)*, *379*, Article 20200267. http://dx.doi.org/10.1098/rsta.2020.0267.

Chamorro, P., Muñiz, C., Levi, R., Arroyo, D., Rodriguez, F. B., & Varona, P. (2012). Generalization of the dynamic clamp concept in neurophysiology and behavior. *PLoS ONE*, *7*(7), http://dx.doi.org/10.1371/journal.pone.0040887.

Chiolerio, A., Chiappalone, M., Ariano, P., & Bocchini, S. (2017). Coupling resistive switching devices with neurons: State of the art and perspectives. *Frontiers in Neuroscience*, *11*, 70. http://dx.doi.org/10.3389/fnins.2017.00070.

Elices, I., Levi, R., Arroyo, D., Rodriguez, F. B., & Varona, P. (2019). Robust dynamical invariants in sequential neural activity. *Scientific Reports*, *9*(1), 9048. http://dx.doi.org/10.1038/s41598-019-44953-2.

Elices, I., & Varona, P. (2015). Closed-loop control of a minimal central pattern generator network. *Neurocomputing*, *170*, 55–62. http://dx.doi.org/10.1016/j.neucom.2015.04.097.

Elices, I., & Varona, P. (2017). Asymmetry factors shaping regular and irregular bursting rhythms in central pattern generators. *Frontiers in Computational Neuroscience*, *11*, 9. http://dx.doi.org/10.3389/fncom.2017.00009.

Frank, J. A., Antonini, M.-J., & Anikeeva, P. (2019). Next-generation interfaces for studying neural function. *Nature biotechnology*, *37*(9), 1013–1023. http://dx.doi.org/10.1038/s41587-019-0198-8.

Garrido-Peña, A., Elices, I., & Varona, P. (2021). Characterization of interval variability in the sequential activity of a central pattern generator model. *Neurocomputing*, *461*, 667–678. http://dx.doi.org/10.1016/j.neucom.2020.08.093.

George, R., Chiappalone, M., Giugliano, M., Levi, T., Vassanelli, S., Partzsch, J., & Mayr, C. (2020). Plasticity and adaptation in neuromorphic biohybrid systems. *iScience*, *23*(10), Article 101589. http://dx.doi.org/10.1016/j.isci.2020.101589.

Ghigliazza, R. M., & Holmes, P. (2004). Minimal models of bursting neurons: How multiple currents, conductances, and timescales affect bifurcation diagrams. *SIAM Journal on Applied Dynamical Systems*, http://dx.doi.org/10.1137/030602307.

Golowasch, J., Casey, M., Abbott, L. F., & Marder, E. (1999). Network stability from activity-dependent regulation of neuronal conductances. *Neural Computation*, *11*(5), 1079–1096. http://dx.doi.org/10.1162/089976699300016359.

Gonçalves, P. J., Lueckmann, J.-M., Deistler, M., Nonnenmacher, M., Öcal, K., Bassetto, G., Chintaluri, C., Podlaski, W. F., Haddad, S. A., Vogels, T. P., Greenberg, D. S., & Macke, J. H. (2020). Training deep neural density estimators to identify mechanistic models of neural dynamics. *ELife*, *9*, Article e56261. http://dx.doi.org/10.7554/eLife.56261.

Hull, T. E., Enright, W. H., Fellen, B. M., & Sedgwick, A. E. (1972). Comparing numerical methods for ordinary differential equations. *SIAM Journal on Numerical Analysis*, *9*(4), 603–637.

Izhikevich, E. (2003). Simple model of spiking neurons. *IEEE Transactions on Neural Networks*, *14*(6), 1569–1572. http://dx.doi.org/10.1109/TNN.2003.820440.

Keren, H., Partzsch, J., Marom, S., & Mayr, C. G. (2019). A biohybrid setup for coupling biological and neuromorphic neural networks. *Frontiers in Neuroscience*, *13*, 432. http://dx.doi.org/10.3389/fnins.2019.00432.

Keren, N., Peled, N., & Korngreen, A. (2005). Constraining compartmental models using multiple voltage recordings and genetic algorithms. *Journal of Neurophysiology*, *94*(6), 3730–3742. http://dx.doi.org/10.1152/jn.00408.2005, PMID: 16093338.

Komendantov, A. O., & Kononenko, N. I. (1996). Deterministic chaos in mathematical model of pacemaker activity in bursting neurons of snail, helix pomatia. *Journal of Theoretical Biology*, *183*, 219–230. http://dx.doi.org/10.1006/jtbi.1996.0215.

Kositsky, M., Chiappalone, M., Alford, S., & Mussa-Ivaldi, S. (2009). Brain-machine interactions for assessing the dynamics of neural systems. *Frontiers in Neurorobotics*, *3*, 1. http://dx.doi.org/10.3389/neuro.12.001.2009.

LaTorre, A., Kwong, M. T., García-Grajales, J. A., Shi, R., Jérusalem, A., & Peña, J.-M. (2020). Model calibration using a parallel differential evolution algorithm in computational neuroscience: Simulation of stretch induced nerve deficit. *Journal of Computer Science*, *39*, Article 101053. http://dx.doi.org/10.1016/j.jocs.2019.101053.

Le Masson, G., Le Masson, S., & Moulins, M. (1995). From conductances to neural network properties: Analysis of simple circuits using the hybrid network method. http://dx.doi.org/10.1016/S0079-6107(96)00004-1.

Le Masson, G., Renaud-Le Masson, S., Debay, D., & Bal, T. (2002). Feedback inhibition controls spike transfer in hybrid thalamic circuits.. *Nature*, *417*(6891), 854–858. http://dx.doi.org/10.1038/nature00825.

Manor, Y., & Nadim, F. (2001). Frequency regulation demonstrated by coupling a model and a biological neuron. *Neurocomputing*, *38–40*, 269–278.

Marder, E., & Calabrese, R. L. (1996). Principles of rhythmic motor pattern generation. *Physiological Reviews*, *76*, 687–717.

Melab, N., Gmys, J., Korosec, P., & Chakroun, I. (2020). Synergy between parallel computing, optimization and simulation. *Journal of Computer Science*, *44*, Article 101168. http://dx.doi.org/10.1016/j.jocs.2020.101168.

Musk, E. (2019). An integrated brain-machine interface platform with thousands of channels. *Journal of Medical Internet Research*, *21*(10), Article e16194. http://dx.doi.org/10.2196/16194.

Nowotny, T., & Varona, P. (2014). Dynamic clamp technique. In *Encyclopedia of computational neuroscience* (pp. 1–4). New York, NY: Springer New York, http://dx.doi.org/10.1007/978-1-4614-7320-6_126-2.

Nowotny, T., Zhigulin, V. P., Selverston, A. I., Abarbanel, H. D. I., & Rabinovich, M. I. (2003). Enhancement of synchronization in a hybrid neural circuit by spike timing dependent plasticity. *Journal of Neuroscience*, *23*, 9776–9785. http://dx.doi.org/10.1523/JNEUROSCI.23-30-09776.2003.

Oprisan, S. A., Prinz, A. A., & Canavier, C. C. (2004). Phase resetting and phase locking in hybrid circuits of one model and one biological neuron. *Biophysical Journal*, *87*(4), 2283–2298. http://dx.doi.org/10.1529/biophysj.104.046193.

Pinto, R. D., Varona, P., Volkovskii, A. R., Szücs, A., Abarbanel, H. D., & Rabinovich, M. I. (2000). Synchronous behavior of two coupled electronic neurons. *Physical Review E - Statistical Physics, Plasmas, Fluids, and Related Interdisciplinary Topics*, *62*(2), 2644–2656. http://dx.doi.org/10.1103/PhysRevE.62.2644.

Potter, S. M. (2002). Hybrots: hybrid systems of cultured neurons+robots, for studying dynamic computation and learning. In *Proceedings of the 2002 simulation of adaptive behavior 7: workshop on motor control in humans and robots-on the interplay of real brains and artificial devices*. Edinburgh, Scotland.

Puebla, H., Hernández-Martínez, E., Rodriguez-Jara, M., & Lopez-Monsalvo, C. S. (2017). Robust master-slave synchronization of neuronal systems. *Mathematical Problems in Engineering*, *2017*, Article 7587294. http://dx.doi.org/10.1155/2017/7587294.

Reyes-Sanchez, M., Amaducci, R., Elices, I., Rodriguez, F. B., & Varona, P. (2020). Automatic adaptation of model neurons and connections to build hybrid circuits with living networks. *Neuroinformaticcs*, *18*, 377–393. http://dx.doi.org/10.1007/s12021-019-09440-z.

Rochford, A. E., Carnicer-Lombarte, A., Curto, V. F., Malliaras, G. G., & Barone, D. G. (2020). When bio meets technology: Biohybrid neural interfaces. *Advanced Materials*, *32*(15), Article 1903182. http://dx.doi.org/10.1002/adma.201903182.

Selverston, A. I. (2005). A neural infrastructure for rhythmic motor patterns. *Cellular and Molecular Neurobiology*, *25*(2), 223–244.

Selverston, A. I., Rabinovich, M. I., Abarbanel, H. D. I., Elson, R., Szücs, A., Pinto, R. D., Huerta, R., & Varona, P. (2000). Reliable circuits from irregular neurons: A dynamical approach to understanding central pattern generators. *Journal of Physiology Paris*, *94*(5–6), 357–374. http://dx.doi.org/10.1016/S0928-4257(00)01101-3.

Serb, A., Corna, A., George, R., Khiat, A., Rocchi, F., Reato, M., Maschietto, M., Mayr, C., Indiveri, G., Vassanelli, S., & Prodromakis, T. (2020). Memristive synapses connect brain and silicon spiking neurons. *Scientific Reports*, *10*(1), 2590. http://dx.doi.org/10.1038/s41598-020-58831-9.

Shi, D., Dhawan, V., & Cui, X. T. (2021). Bio-integrative design of the neural tissue-device interface. *Current Opinion in Biotechnology*, *72*, 54–61. http://dx.doi.org/10.1016/j.copbio.2021.10.003.

Soëtard, P., Amaducci, R., Sánchez-Martín, P., Reyes-Sanchez, M., Garrido-Peña, A., Levi, R., F.B., R., & Varona, P. (2023). Dynamical principles of functional neural sequences validated in hybrid robots built with living central pattern generators. *Journal of Computational Neuroscience*, *51 (Suppl 1)*, 3–101 P110. http://dx.doi.org/10.1007/s10827-022-00841-9.

Szücs, A., Varona, P., Volkovskii, A. R., Abarbanel, H. D. I., Rabinovich, M. I., & Selverston, A. I. (2000). Interacting biological and electronic neurons generate realistic oscillatory rhythms. *Neuroreport*, *11*(3), 563–569. http://dx.doi.org/10.1097/00001756-200002280-00027.

Tennøe, S., Halnes, G., & Einevoll, G. T. (2018). Uncertainpy: A python toolbox for uncertainty quantification and sensitivity analysis in computational neuroscience. *Frontiers in Neuroinformatics*, *12*, 49. http://dx.doi.org/10.3389/fninf.2018.00049.

Torres, J. J., Baroni, F., Latorre, R., & Varona, P. (2020). Temporal discrimination from the interaction between dynamic synapses and intrinsic subthreshold oscillations. *Neurocomputing*, *417*, 543–557. http://dx.doi.org/10.1016/j.neucom.2020.07.031.

Torres, J. J., Uzuntarla, M., & Marro, J. (2020). A theoretical description of inverse stochastic resonance in nature. *Communications in Nonlinear Science and Numerical Simulation*, *80*, Article 104975. http://dx.doi.org/10.1016/j.cnsns.2019.104975.

Torres, J. J., & Varona, P. (2012). Modeling biological neural networks. *Vol. 1–4*, In *Handbook of natural computing* (pp. 533–564). Berlin, Heidelberg: Springer, http://dx.doi.org/10.1007/978-3-540-92910-9_17.

Van Geit, W., Gevaert, M., Chindemi, G., Rössert, C., Courcol, J.-D., Muller, E. B., Schürmann, F., Segev, I., & Markram, H. (2016). BluePyOpt: Leveraging open source software and cloud infrastructure to optimise model parameters in neuroscience. *Frontiers in Neuroinformatics*, *10*, 17. http://dx.doi.org/10.3389/fninf.2016.00017.

Vanier, M. C., & Bower, J. M. (1999). A comparative survey of automated parameter-search methods for compartmental neural models. *Journal of Computational Neuroscience*, *7*(2), 149–171. http://dx.doi.org/10.1023/A:1008972005316.

Varona, P., Arroyo, D., Rodriguez, F. B., & Nowotny, T. (2016). Online event detection requirements in closed-loop neuroscience. In A. E. Hady (Ed.), *Closed loop neuroscience* (pp. 81–91). San Diego: Academic Press, http://dx.doi.org/10.1016/B978-0-12-802452-2.00006-8.

Varona, P., Ibarz, J., López-Aguado, L., & Herreras, O. (2000). Macroscopic and subcellular factors shaping population spikes. *Journal of Neurophysiology*, *83*(4), 2192–2208. http://dx.doi.org/10.1152/jn.2000.83.4.2192.

Varona, P., Torres, J., Huerta, R., Abarbanel, H., & Rabinovich, M. (2001). Regularization mechanisms of spiking-bursting neurons. *Neural Networks*, *14*(6–7), 865–875. http://dx.doi.org/10.1016/S0893-6080(01)00046-6.

Vassanelli, S., & Mahmud, M. (2016). Trends and challenges in neuroengineering: Toward "intelligent" neuroprostheses through brain-"brain inspired systems" communication. *Frontiers in Neuroscience*, *10*, 438. http://dx.doi.org/10.3389/fnins.2016.00438.

Wan, C., Cai, P., Guo, X., Wang, M., Matsuhisa, N., Yang, L., Lv, Z., Luo, Y., Loh, X. J., & Chen, X. (2020). An artificial sensory neuron with visual-haptic fusion. *Nature Communications*, *11*(1), 4602. http://dx.doi.org/10.1038/s41467-020-18375-y.

Xia, B., Sebesta, C., Lee, S., Nair, V., Zhao, X., Coffler, S., Robinson, J. T., & Szablowski, J. O. (2021). Biohybrid approaches to interface with the nervous system: the best of both worlds. *Current Opinion in Biotechnology*, *72*, 86–94. http://dx.doi.org/10.1016/j.copbio.2021.10.009.

Yarom, Y. (1991). Rhythmogenesis in a hybrid system-interconnecting an olivary neuron to an analog network of coupled oscillators. *Neuroscience*, *44*(2), 263–275.

Zaer, H., Deshmukh, A., Orlowski, D., Fan, W., Prouvot, P.-H., Glud, A. N., Jensen, M. B., Worm, E. S., Lukacova, S., Mikkelsen, T. W., Fitting, L. M., Adler, J. R., Schneider, M. B., Jensen, M. S., Fu, Q., Go, V., Morizio, J., Sørensen, J. C. H., & Stroh, A. (2021). An intracortical implantable brain-computer interface for telemetric real-time recording and manipulation of neuronal circuits for closed-loop intervention. *Frontiers in Human Neuroscience*, *15*, Article 618626. http://dx.doi.org/10.3389/fnhum.2021.618626.

Zeck, G., & Fromherz, P. (2001). Noninvasive neuroelectronic interfacing with synaptically connected snail neurons immobilized on a semiconductor chip. *Proceedings of the National Academy of Sciences*, *98*(18), 10457–10462. http://dx.doi.org/10.1073/pnas.181348698.

Zirkle, J., & Rubchinsky, L. L. (2021). Noise effect on the temporal patterns of neural synchrony. *Neural Networks*, *141*, 30–39. http://dx.doi.org/10.1016/j.neunet.2021.03.032.